A comparative study of the capacity of mesenchymal stromal cell lines to form spheroids

Margaux Deynoux, Nicola Sunter, Elfi Ducrocq, Hassan Dakik, Roseline Guibon, Julien Burlaud-Gaillard, Lucie Brisson, Florence Rouleux-Bonnin, Louis-Romée Le Nail, Olivier Herault, et al.

PLOS ONE

RESEARCH ARTICLE

A comparative study of the capacity of mesenchymal stromal cell lines to form spheroids

Margaux Deynoux[1☯], Nicola Sunter[1☯], Elfi Ducrocq[1], Hassan Dakik[1], Roseline Guibon[2,3], Julien Burlaud-Gaillard[4,5], Lucie Brisson[3], Florence Rouleux-Bonnin[1], Louis-Romée le Nail[6], Olivier Hérault[1,7], Jorge Domenech[1,7], Philippe Roingeard[4,5], Gaëlle Fromont[2,3], Frédéric Mazurier[1]*

1 EA 7501 GICC, CNRS ERL 7001 LNOx, Université de Tours, Tours, France, **2** Anatomie et cytologie pathologique, CHRU de Tours, Tours, France, **3** INSERM UMR1069, Nutrition, Croissance et Cancer, Université de Tours, Tours, France, **4** Plateforme IBiSA de Microscopie Electronique, Université et CHRU de Tours, Tours, France, **5** INSERM U1259 MAVIVH, Université et CHRU de Tours, Tours, France, **6** Service de Chirurgie orthopédique, CHU Tours, Tours, France, **7** Service d'hématologie biologique, CHRU de Tours, Tours, France

☯ These authors contributed equally to this work.
* frederic.mazurier@inserm.fr

Citation: Deynoux M, Sunter N, Ducrocq E, Dakik H, Guibon R, Burlaud-Gaillard J, et al. (2020) A comparative study of the capacity of mesenchymal stromal cell lines to form spheroids. PLoS ONE 15 (6): e0225485. https://doi.org/10.1371/journal.pone.0225485

Editor: Atsushi Asakura, University of Minnesota Medical School, UNITED STATES

Received: October 30, 2019

Accepted: May 17, 2020

Published: June 2, 2020

Peer Review History: PLOS recognizes the benefits of transparency in the peer review process; therefore, we enable the publication of all of the content of peer review and author responses alongside final, published articles. The editorial history of this article is available here: https://doi.org/10.1371/journal.pone.0225485

Data Availability Statement: All relevant data are within the paper and its Supporting Information files.

Abstract

Mesenchymal stem cells (MSC)-spheroid models favor maintenance of stemness, *ex vivo* expansion and transplantation efficacy. Spheroids may also be considered as useful surrogate models of the hematopoietic niche. However, accessibility to primary cells, from bone marrow (BM) or adipose tissues, may limit their experimental use and the lack of consistency in methods to form spheroids may affect data interpretation. In this study, we aimed to create a simple model by examining the ability of cell lines, from human (HS-27a and HS-5) and murine (MS-5) BM origins, to form spheroids, compared to primary human MSCs (hMSCs). Our protocol efficiently allowed the spheroid formation from all cell types within 24 hours. Whilst hMSC-spheroids began to shrink after 24 hours, the size of spheroids from cell lines remained constant during three weeks. The difference was partially explained by the balance between proliferation and cell death, which could be triggered by hypoxia and induced oxidative stress. Our results demonstrate that, like hMSCs, MSC cell lines make reproductible spheroids that are easily handled. Thus, this model could help in understanding mechanisms involved in MSC functions and may provide a simple model by which to study cell interactions in the BM niche.

Introduction

Over the last two decades, extensive studies have attempted to characterize mesenchymal stem cell (MSC). Initially described in the bone marrow (BM), MSCs were later found in almost all adult and fetal tissues [1]. Their classification rapidly suffered from a lack of clear phenotypical definition. Therefore, in 2006, the International Society for Cellular Therapy (ISCT) defined

Funding: The authors acknowledge the Ministry of Research (MD), the ARC Foundation (MD, HD), the French Society of Hematology (MD), the "Ligue contre le Cancer (NS)", and the Lebanese south governate (HD) for their funding. This work was supported by the French Committees of the "Ligue Contre le Cancer Grand-Ouest" [16 (Charente), 36 (Indre), 37 (Indre-et-Loire), 41 (Loire et Cher), and 86 (Vendée)] and the Région Centre Val de Loire (FM). The funders had no role in study design, data collection and analysis, decision to publish, or preparation of the manuscript.

Competing interests: The authors have declared that no competing interests exist.

MSCs according to three minimal criteria: adherence to plastic, specific cell surface markers and multipotent potential. Indeed, MSCs are classically described as stem cells that are able to differentiate into osteoblasts, adipocytes and chondroblasts [2], making them an attractive source of cells in regenerative medicine. Subsequent studies have also established their ability to differentiate into cardiomyocytes [3], neurons [4], epithelial cells [5] and hepatocytes [6]. The discovery of the multiple functions of MSC, such as those involved in the anti-inflammatory response [7] and in injury repair [8,9] confirmed them as promising cellular tools in regenerative medicine.

Furthermore, MSCs represent a key component of the BM microenvironment supporting normal hematopoiesis through the regulation of stem cell renewal and differentiation processes, but also fueling malignant cells and protecting them from therapeutic agents [10]. As such, primary MSCs have often been used as feeder layers in long-term co-culture of hematopoietic cells *in vitro* in preclinical studies [11]. With the aim of standardization, the murine MS-5 cell line became a standard for both normal or malignant hematopoietic cell culture [12]. This robust co-culture model has been widely used and has contributed to the characterization of hematopoietic stem cells (HSC) [11]. This two-dimensional (2D) system, while closer to BM physiology than the culture of hematopoietic cells alone, still lacks the three-dimensional (3D) complexity of the BM niche. Thus, although widely used, it is certainly not sufficiently consistent at predicting *in vivo* responses [13]. Therefore, a 3D system might be a better alternative to mimic the BM microenvironment.

Critically, the culture leads to rapid loss of MSC pluripotency and supportive functions. Therefore, a wide range of techniques to form 3D MSCs aggregates, from the simplest spheroids to the more complex matrix-based structures, have been proposed [14]. Studies of spheroids, also called mesenspheres, were mostly dedicated to the examination of MSC stemness and differentiation abilities, such as osteogenesis, in order to improve their *in vitro* expansion and transplantation efficacy in regenerative medicine [15,16]. Furthermore, this model has also been tested as a surrogate niche for hematopoietic cells [17–23]. Spheroids take advantage of the ability of MSCs to self-aggregate, which is improved by using various approaches such as low adhesion plates, natural and artificial (centrifugation) gravity, cell matrix or more complex scaffolds [13,14,24,25]. Classically, studies have used human primary MSCs, from BM, cord blood and lipoaspirate, or rodent sources [15,26].

Although immortalized MSCs, or well characterized cell lines, could bypass the lack of primary cells and avoid the variability involved with use of primary human MSCs (hMSCs) samples, they are rarely employed to make spheroids [27,28]. Cell lines would also allow better standardization of the spheroid formation protocol. In this study, we examined the spheroid-forming capacity of two human cell lines (HS-27a and HS-5) and the currently used murine MS-5 cell line, in comparison with primary hMSCs. We defined a simple and fast method using standard matrix to form spheroids and characterized them in terms of physical features, cell proliferation and death.

Materials and methods

Cell culture and reagents

The murine MS-5 bone marrow (BM) stromal cell line was kindly provided by Mori KJ (Niigata University, Japan) [29]. HS-27a and HS-5 human BM stromal cell lines were purchased from American Type Culture Collection (CRL-2496 and CRL-11882, respectively). Primary BM hMSCs were obtained by iliac crest aspiration from healthy donors (without hematological disorders) undergoing orthopedic surgery at the University Hospital of Tours, after informed consent, for cell banking according to the Declaration of Helsinki, as approved by the French

Ministry of Education and Research (authorization number No. DC-2008-308). Samples from BM aspirates were diluted in MEM Alpha (Life Technologies, Villebon-sur-Yvette, France) and filtered through a cell-strainer prior to centrifugation (350 x g, 10 min). Cells were resuspended and seeded at 10^5 to 2.10^5 cells/cm^2 in MEM Alpha supplemented with 100 U/mL penicillin and 100 μg/mL streptomycin (both from Life Technologies) and 1 ng/mL of recombinant human FGF basic (FGF-2, R&D Systems, Abingdon, United Kingdom). Medium was changed twice a week until cells reached confluency. In experiments, primary hMSCs were used at passage 2. HS-27a and HS-5 cell lines were cultured in RPMI 1640 (Life Technologies) and MS-5 in MEM Alpha. All media were supplemented with 10% heat-inactivated fetal bovine serum (FBS), 2 mM L-glutamine (Life Technologies), 100 U/mL penicillin and 100 μg/mL streptomycin. Cells were maintained in a saturated humidified atmosphere at 37˚C and 5% CO_2.

Spheroids formation

For one spheroid, 30,000 cells were cultured in 100 μL of medium, supplemented by 0.25% to 1% of either Methocult^{TM} H4100 or SF H4236 (StemCell, Grenoble, France), and seeded in U-bottomed 96-well plate (Sarstedt, Marnay, France). Both media contains methylcellulose in IMDM, but SF H4236 is supplemented with bovine serum albumin, recombinant human insulin, human transferrin (iron-saturated), 2-Mercaptoethanol and unknown supplements as described by the manufacturer. The medium was the same as that of the normal culture for each cell line but supplemented with heat inactivated FBS to reach 15%. At days as detailed, microscopic analysis was performed using a Leica DMIL microscope (Leica, Nanterre, France), coupled to a DXM1200F camera (Nikon, Champigny-sur-Marne, France). To determine the number of cells in each spheroid over time, only wells with a unique, fully-formed spheroid were selected. Twelve spheroids per experiment were pooled and dissociated with 2 mg/mL collagenase 1A (Sigma-Aldrich, Saint-Quentin-Fallavier, France), 10 min at 37˚C, with agitation every two minutes, and then counted by the trypan blue exclusion assay.

Time-lapse video

Automatic acquisitions were performed on a Nikon Eclipse TI-S microscope, coupled to a DS Qi2 camera (Nikon). The system includes a cage incubator (Okolab, Pozzuoli, NA, Italy) controlling temperature and level of CO_2. Analyses were performed using both NIS Element BR (Nikon) and Fiji/ImageJ softwares.

Scanning electron microscopy

Spheroids were fixed by incubation for 24 h in 4% paraformaldehyde, 1% glutaraldehyde in 0.1 M phosphate buffer (pH 7.2). Samples were then washed in phosphate-buffered saline (PBS) and post-fixed by incubation with 2% osmium tetroxide for 1 h. Spheroids were then fully dehydrated in a graded series of ethanol solutions, and dried in hexamethyldisilazane (HMDS, Sigma-Aldrich). Finally, samples were coated with 40 Å platinum, using a PECS 682 apparatus (Gatan, Evry, France), before observation under an Ultra plus FEG-SEM scanning electron microscope (Zeiss, Marly-le-Roi, France).

Transmission electron microscopy

Spheroids were fixed by incubation for 24 h in 4% paraformaldehyde, 1% glutaraldehyde in 0.1 M phosphate buffer (pH 7.2). Samples were then washed in phosphate-buffered saline (PBS) and post-fixed by incubation with 2% osmium tetroxide for 1 h. Spheroids were then fully

dehydrated in a graded series of ethanol solutions and propylene oxide. Impregnation step was performed with a mixture of (1:1) propylene oxide/Epon resin, and then left overnight in pure resin. Samples were then embedded in Epon resin, which was allowed to polymerize for 48 h at 60˚C. Ultra-thin sections (90 nm) were obtained with an EM UC7 ultramicrotome (Leica). Sections were stained with 5% uranyl acetate (Agar Scientific, Stansted, United Kingdom), 5% lead citrate (Sigma-Aldrich) and observations were made with a transmission electron microscope (Jeol, JEM 1011, Croissy-sur-Seine, France).

Immunohistochemistry

At least five spheroids per condition were pooled, fixed in formalin, embedded in paraffin and cut in 3–4 μm sections on Superfrost Plus slides. Slides were deparaffinized, rehydrated and heated in citrate buffer pH 6 for antigenic retrieval. After blocking for endogenous peroxidase with 3% hydrogen peroxide, the primary antibodies were incubated. The panel of primary antibodies included anti-HIF-1α (Abcam ab51608, Paris, France) (dilution 1/200, incubation 1 h), anti-VEGF-A (Abcam ab1316, dilution 1/200, incubation 1 h), anti-HO-1 (Abcam ab52947, dilution 1/1 000, incubation 1 h), anti-CA-IX (Novocastra clone TH22, Nanterre, France) (dilution 1/100, incubation 20 min), anti-Ki-67 (DakoCytomation clone 39–9, Glostrup, Denmark) (dilution 1/50, incubation 30 min), anti-caspase 3 (Novocostra clone JHM62, Nanterre, France) (dilution 1/100, incubation 1 h) and anti-LC3B (Novus Biological NB 600–1384, Cambridge, UK) (dilution 1/200, incubation 1 h). Immunohistochemistry was performed with either the automated BenchMark XT slide stainer (Ventana Medical System Inc.) using OptiView Detection Kit (Ventana Medical System Inc.) (for CA-IX and Ki-67), or manually using the streptavidin-biotin-peroxidase method with diaminobenzidine as the chromogen (Kit LSAB, DakoCytomation). Slides were finally counterstained with haematoxylin. Negative controls were obtained after omission of the primary antibody or incubation with a non-specific antibody.

Quantitative real-time PCR

Total RNAs were extracted using TRIzol reagent (Life Technologies) and reverse transcription was performed with the SuperScript™ VILO™ cDNA Synthesis Kit (Invitrogen, Villebon-sur-Yvette, France), both according to the manufacturer's procedures. qRT-PCR was performed on a LightCycler® 480 (Roche, Switzerland) with the LightCycler® 480 Probes Master (Roche). *GAPDH*, *ACTB*, *RPL13A* and *EF1A* genes were used as endogenous genes for normalization. Primer sequences (S1 Table) were designed with the ProbeFinder software (Roche), and all reactions were run in triplicate.

Cell cycle analysis

Spheroids were dissociated with 2 mg/mL collagenase 1A (Sigma-Aldrich), 10 min, at 37˚C, with agitation every two minutes. Cells were fixed with 2% paraformaldehyde/0.03% saponin for 15 min at room temperature (RT), and washed three times for 5 min with 10% FBS/0.03% saponin. Cells were then stained with 7-Aminoactinomycin D (7-AAD, Sigma-Aldrich) and an AF488-conjugated anti-KI-67 antibody (BD Biosciences, Le Pont de Claix, France) or the AF488-conjugated IgG_1 isotype control (BD Biosciences). Experiments were performed on an Accuri™ C6 flow cytometer (BD Biosciences) and data were analyzed with the FlowJo V10.4.1 software (Tree Star Inc.).

Statistical analysis

All statistical analyses were performed using R software. Since our sampling never exceeds n = 6, we used nonparametric tests. The Mann-Whitney test was used to compare two conditions and Kruskal-Wallis for multiple comparisons, followed by a Dunn's *post hoc* test. The threshold for significance was set up to a p-value of 0.05.

Results

Establishment of primary hMSC-spheroids by cell aggregation method

From the different methods to form MSC-spheroids, we followed an approach based on cell aggregation in methylcellulose-based medium [27]. To establish a protocol that is simple, reproducible and compatible with hematopoietic cell culture, two commercial methylcelluloses (MethoCult H4100 and SF H4236) developed for hematopoietic progenitors assays were tested (Fig 1A). A range from 0.01 to 1% of methylcellulose has been previously used [27,30–33], so we tested three different concentrations (0.25, 0.5 and 1%). We also tested the hanging drop technique [31,33–35] and the previously described U-bottomed 96-well plates methods [27,30,32,33,36]. Both techniques worked well for primary hMSCs but the second was more appropriate for further analyses since the handling is easier and the volume of medium higher, which could prevent starvation and dehydration in long-term cultures. The SF H4236 methylcellulose at a concentration of 0.5% was adopted because it generated only one spheroid in most of the wells with lower condensation aspect for primary hMSCs (Fig 1B). Under these culture conditions, MSCs were able to form spheroids rapidly, in as little as five hours of culture (S1 Video), which is consistent with previous studies [27,32,37].

Formation of spheroids from MSC lines

The spheroid-forming capacity was followed for two human cell lines, HS-27a and HS-5, and compared to that of primary hMSCs. The two cell lines were obtained by immortalization of hMSCs from the same BM sample with the papilloma virus E6/E7 genes [38,39]. HS-27a cells support hematopoietic stem cell maintenance (self-renewal, formation of cobblestone areas), whereas HS-5 cells mainly sustain proliferation and differentiation [38–40]. Like primary hMSCs, they both retained the ability to form spheres but required about 10 hours to make rounded spheroids (S2 and S3 Videos). Although cells of various origins formed spheroids of equivalent sizes (about 300 μm of diameter) after 24 hours, primary hMSC-spheroids rapidly condensed and reached half of their initial perimeter after 14 days of culture (Fig 2A and 2B). In contrast to primary hMSCs, the perimeter of spheroids resulting from both cell lines remained constant during three weeks. Knowing that primary hMSCs and cell lines may differ in their growth properties, we used the murine MS-5 cell line that has contact inhibition [29]. This cell line was able to quickly form spheroids similarly to the other cell lines (S4 Video). It is noteworthy that MS-5 cells initially formed a flat multilayer disk of cells prior to contracting into spheres. Similarly to the spheroids from human cell lines, spheroids from MS-5 cells kept the same size over time (Fig 2A and 2B). This suggests that shrinking might be an intrinsic property or extracellular matrix (ECM) composition of primary cells rather than related to cell proliferation control. We thus examined whether the difference in the size maintenance between various MSCs might be attributed to the cell number per spheroid. In order to quantify the viable cells, spheroids were dissociated at different timepoints after seeding. In accordance with the decrease in circumference, the number of cells per spheroid from primary hMSCs dramatically dropped within seven days (Fig 2C), in agreement with other studies [31,35]. Remarkably, although keeping the same size, HS-27a-spheroids, as well as the MS-5

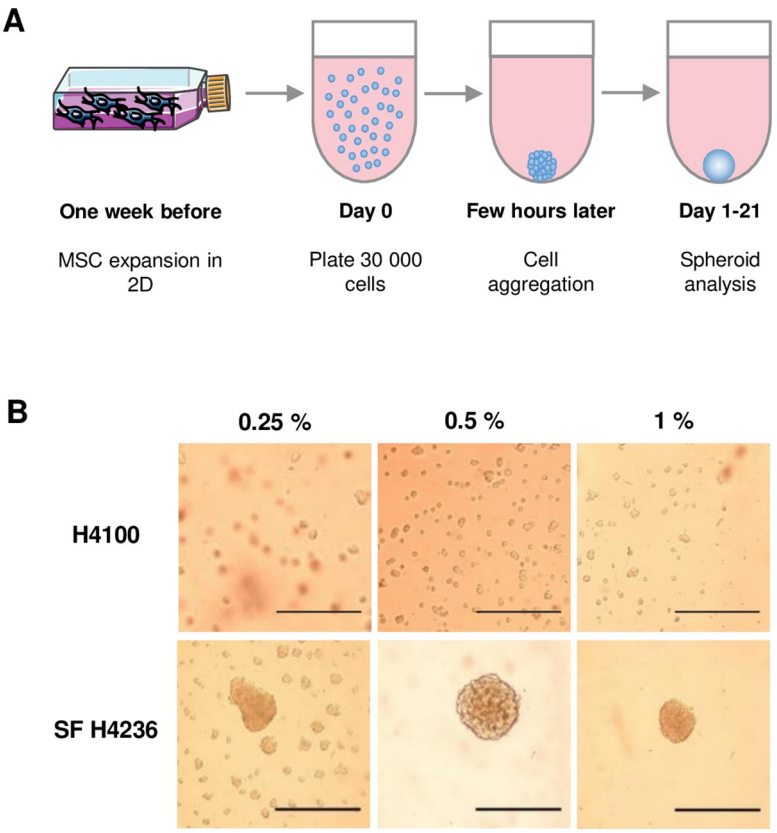

Fig 1. Spheroids formation from primary hMSCs. (A) Schematic representation of experimental plan. (B) 30,000 primary hMSCs per well were seeded into U-bottomed 96-well in medium containing 0.25%, 0.5% or 1% of methylcellulose (Methocult^{TM} H4100 or SF H4236). Microscopy analysis was performed after 24 h (scale bars = 500 μm).

https://doi.org/10.1371/journal.pone.0225485.g001

ones, had lost viable cells similarly to primary hMSCs (Fig 2C). In contrast, HS-5-spheroids had less obvious decrease in cell number with time (Fig 2C). Overall, the size reduction does not seem to be strictly attributable to reduced cell number in spheroids and could be possibly attributed to other factors such as the ECM composition.

Electron microscopy observation of the MSC-spheroids

Scanning electron microscopy (SEM) confirmed the shrinking of primary hMSC-spheroids (Fig 3A and S1A Fig). SEM also revealed, at higher magnification, that spheroids from primary hMSCs are highly cohesive, showing tight intercellular connections forming a flat surface, whereas HS-27a- and HS-5-spheroids, and to a lesser extend MS5-spheroids, exhibited more rounded cells at their surface (Fig 3B and S1B Fig). This phenomenon intensified over time and may explain the size reduction of hMSC-spheroids compared to the cell lines. Absence of ECM is not involved, since ECM deposition is visible for all cell types (Fig 3B). From day 7 for cell lines and day 14 for primaries, spheroid structure began to change, showing loss of cell-cell adhesion, and cell death at the surface.

Further analysis by transmission electron microscopy (TEM) was performed to investigate the ultrastructure of the cells within the spheroids. Between day 1 and day 7, cells showed the swelling of the cell cytoplasm and the presence of an increasing number of necrotic cells, thus suggesting particularly rapid induction of cell death for primary hMSCs compared to cell lines

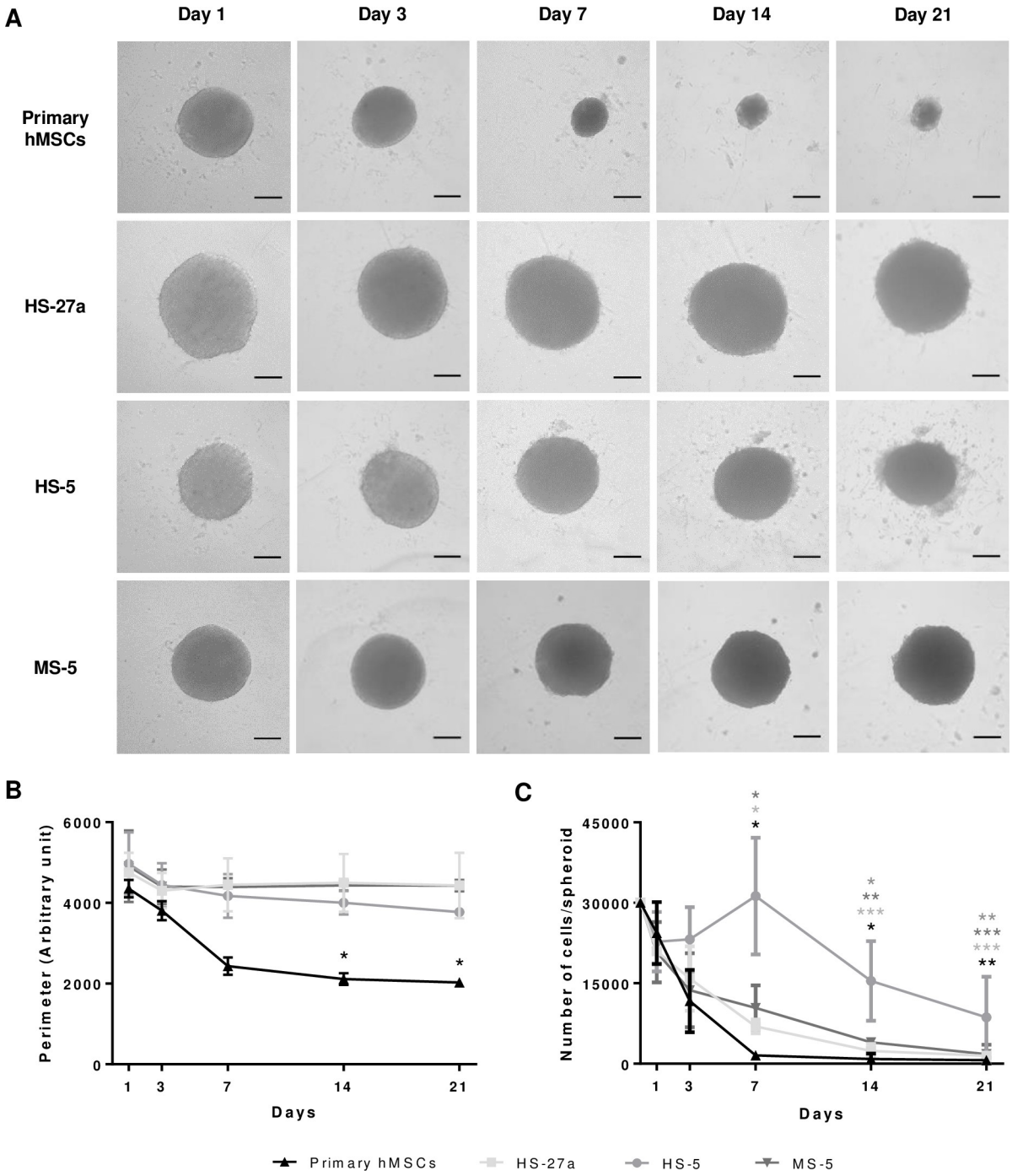

Fig 2. Follow up of the spheroids from various MSCs. (A) Microscopy analysis of primary hMSC-, HS-27a-, HS-5- and MS-5-spheroids over 21 days in culture (scale bars = 100 μm). (B) Perimeter was measured with an arbitrary unit; each experiment is the mean of at least 10 spheroids from n = 3 experiments. Data are shown as mean ± SD; * compared to day 1; * $p \leq 0.01$. (C) Number of living cells per spheroid over 21 days in culture (primary hMCSs and MS-5 n = 3; HS-27a and HS-5 n = 4). Data are shown as mean ± SD; *, **, *** compared to day 0; * $p \leq 0.05$; ** $p \leq 0.01$; *** $p \leq 0.001$.

https://doi.org/10.1371/journal.pone.0225485.g002

(S2A–S2L Fig). Strong induction of autophagy, indicative of cell stress, was demonstrated by appearance of numerous cytoplasmic vacuoles and autophagosomes for primary hMSCs, as soon as day 1 (S2A Fig), and could certainly explain the shrinking. Remarkably, despite a

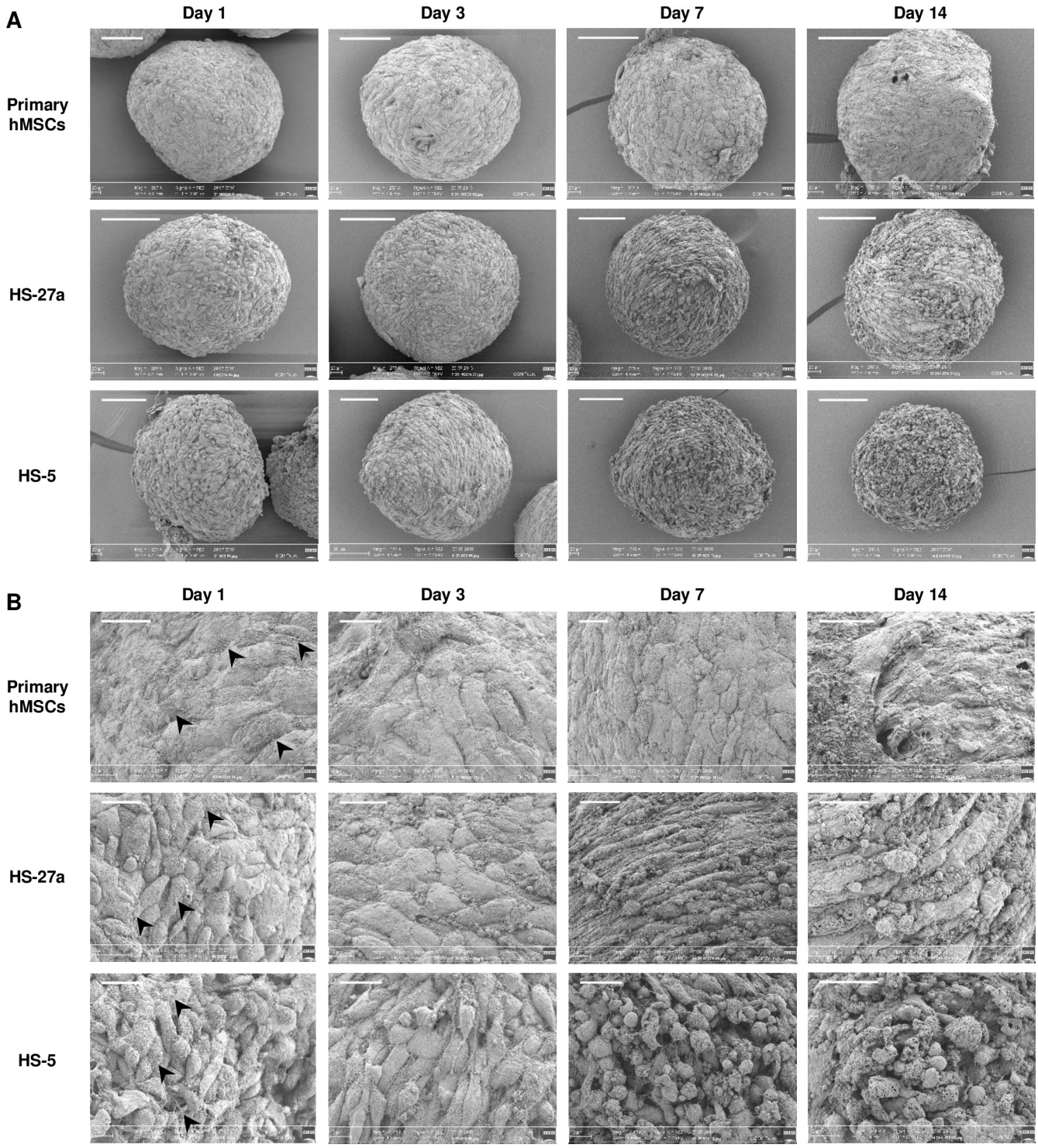

Fig 3. Scanning electron microscopy (SEM) observation of MSC-spheroids. (A) Spheroids from primary hMSCs are round with a smooth surface and show progressive shrinking. HS-27a- and HS-5-spheroids are more irregular and granular. (B) Higher magnification show that cells are cohesive at the surface of primary hMSC-spheroids and more chaotic with distinguishable cells of different shapes for human cell lines. ECM deposition (arrow heads) is visible on all spheroids. Scale bars = 100 μm (A) and 20 μm (B).

https://doi.org/10.1371/journal.pone.0225485.g003

higher apparent loss of cell adhesion by TEM, induction of cell death (necrosis) appeared delayed for cell lines. In addition, although the number of cytoplasmic vacuoles increased over time, no autophagosomes were noted in cell lines. Consistent with this observation, although LC3B expression can be triggered in HS-27a cells (S3 Fig), its subcellular expression remains uniformly cytoplasmic rather than as dot-like staining patterns, which may thus indicate a block in the autophagic mechanism as previously described [41,42].

Cell death and proliferation of the MSC-spheroids

To explain why spheroids showed decreased cell number over time, we proposed an imbalance between cell death and cell proliferation. Cell death has already been noted by electronic microscopy observation though autophagy and cell lysis. Apoptosis and cell cycle were first determined by flow cytometry using 7-AAD/Ki-67 staining (Fig 4A). Increasing sub-G_0/G_1 cell population revealed a strong induction of necrosis and/or late apoptosis after 14 days in hMSC-spheroids, whereas none or moderate cell death was observed for the two human cell lines (Fig 4B). In accordance with these data, caspase-3 staining showed few apoptotic cells until day 7 for primary hMSCs and HS-5 cells (Fig 4C). In contrast, apoptosis in HS-27a-spheroids was observed as soon as day 1, and increased with time, which is consistent with earlier detection of death cells by flow cytometry (Fig 4B). Regarding the proliferation, although harvested at the same confluency, primary hMSCs appeared already much more quiescent than HS-27a or HS-5 cells at day 0 (Fig 4D). A significant proportion of cells remained proliferating in spheroids until day 3 for HS-27a and day 7 for HS-5 cells. Remarkably, while closer to HS-27a cells in terms of perimeter and number of cells, MS-5 cells had a massive increase in cell death and almost no proliferation (S1C and S1D Fig), similarly to primary hMSCs. Ki-67 detection by immunochemistry, in primary hMSCs and human cell lines, revealed homogeneous staining at day 1 indicating proliferation in the whole spheroid (Fig 4E) in agreement with a previous study [43]. Staining confirmed a lower proliferation rate of primary hMSCs compared to cell lines and a rapid proliferation arrest with only few Ki-67-positive cells remaining at the periphery of the spheroid at day 3. A progressive decrease in proliferation for the human cell lines supported the results obtained by flow cytometry. Remarkably, decreased proliferation appears in the entire spheroid and is not restricted to in-depth localizations. These data showed that spheroids are characterized by imbalance between cell death and proliferation, which may explain the highest loss of cells over time.

Hypoxia and oxidative stress in MSC-spheroids

Like in tumor spheres [44–46], the appearance of an oxygen gradient and hypoxia in MSC-spheroids has been demonstrated [47,48]. Carbonic anhydrase IX (CA-IX), a mediator of hypoxia-induced stress response, is commonly used as marker in tumors [49]. Increased CA-IX has been observed in MSC-spheroids, particularly for HS-27a cells (Fig 5A). The pro-survival adaptation to hypoxia occurs mainly through the stabilization of the hypoxia-inducible factors (HIFs). HIFs are key regulators of multiple cell processes, including cell cycle, metabolism, pH control and autophagy. Increasing expression of HIF-1α protein expression has been observed in spheroids over time, as well as at the mRNA level (Fig 5B). Finally, we examined the expression of *VEGFA*, a typical HIF transcriptionally regulated gene [50]. Its expression in hMSC- and HS-27a-spheroids was already elevated at day 1, but strongly increased at both protein and mRNA levels over time (Fig 5C).

In certain circumstances, very low level of oxygen (anoxia) or long exposure to hypoxia may provoke DNA damage and oxidative stress that trigger apoptosis [44,46]. Besides hypoxia appearance in spheroids, cell aggregation may also stress the cells by itself and increase reactive

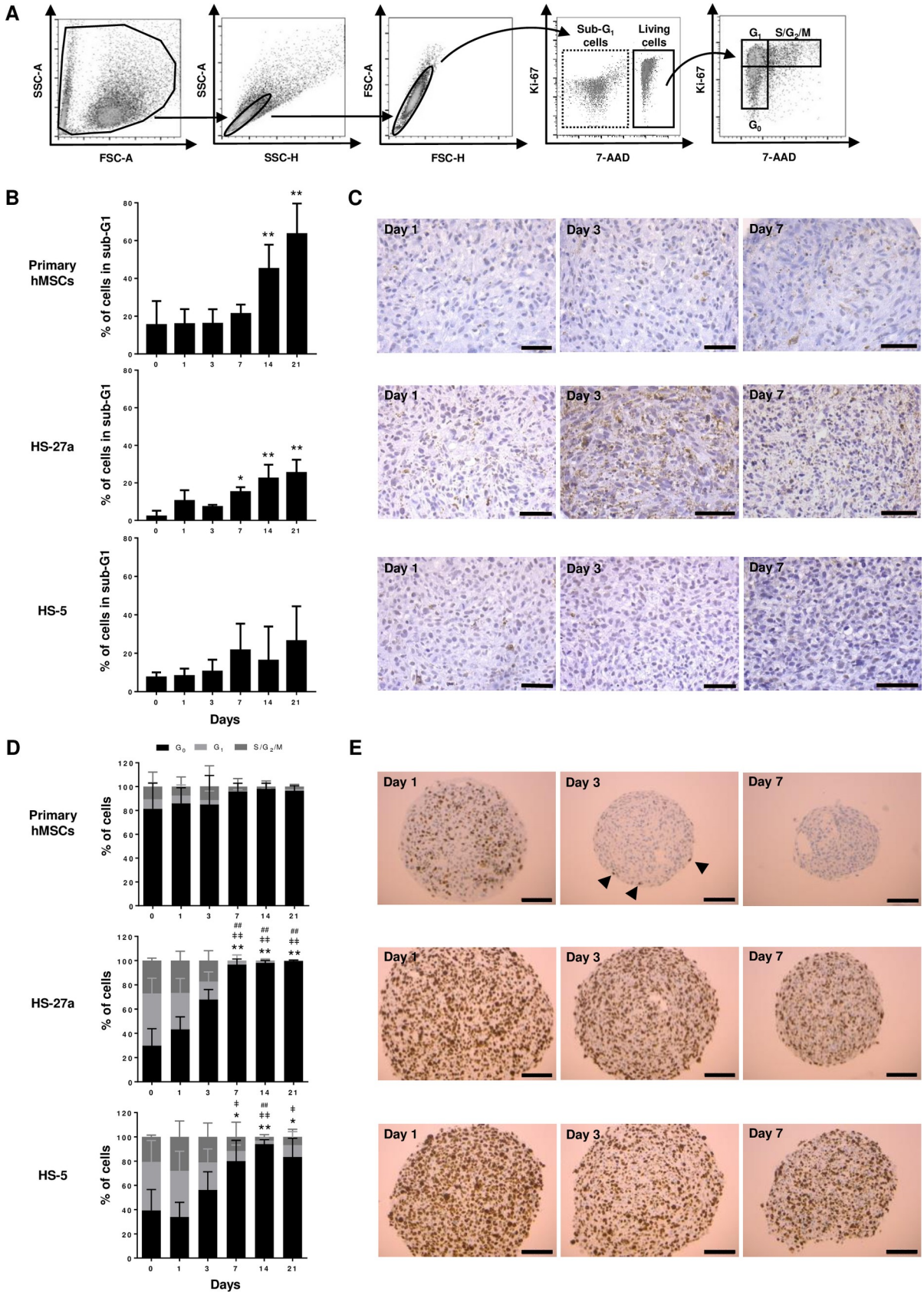
A
SSC-A
FSC-A
SSC-A
SSC-H
FSC-A
FSC-H
Sub-G1 cells
Living cells
Ki-67
7-AAD
G1
S/G2/M
G0
Ki-67
7-AAD
B
Primary hMSCs
HS-27a
HS-5
% of cells in sub-G1
Days
C
Day 1
Day 3
Day 7
D
G0
G1
S/G2/M
Primary hMSCs
HS-27a
HS-5
% of cells
Days
E
Day 1
Day 3
Day 7

Fig 4. Determination of proliferation and apoptosis of MSC-spheroids. (A, B and D) Cell cycle analysis of spheroids over 21 days in culture. (A) Representative gating strategy from primary hMSCs at day 0, (B) sub-G_1 apoptosis quantification (primary hMSCs n = 6; HS-27a and HS-5 n = 3) and (D) cell cycle quantification (primary hMSCs n = 6; HS-27a and HS-5 n = 5; * for G_0; ǂ for G_1; # for S/G_2/M) (data are mean ± SD; *, ǂ, # compared to day 0; *, ǂ $p \leq 0.05$; **, ǂǂ, ## $p \leq 0.01$). (C and E) Immunohistochemistry of (C) caspase-3 and (E) Ki-67 at days 1, 3 and 7 for primary hMSC-, HS-27a- and HS-5-spheroids (scale bars = 50 μm (C) and 100 μm (E)). Arrow heads indicate Ki-67-positive cells.

https://doi.org/10.1371/journal.pone.0225485.g004

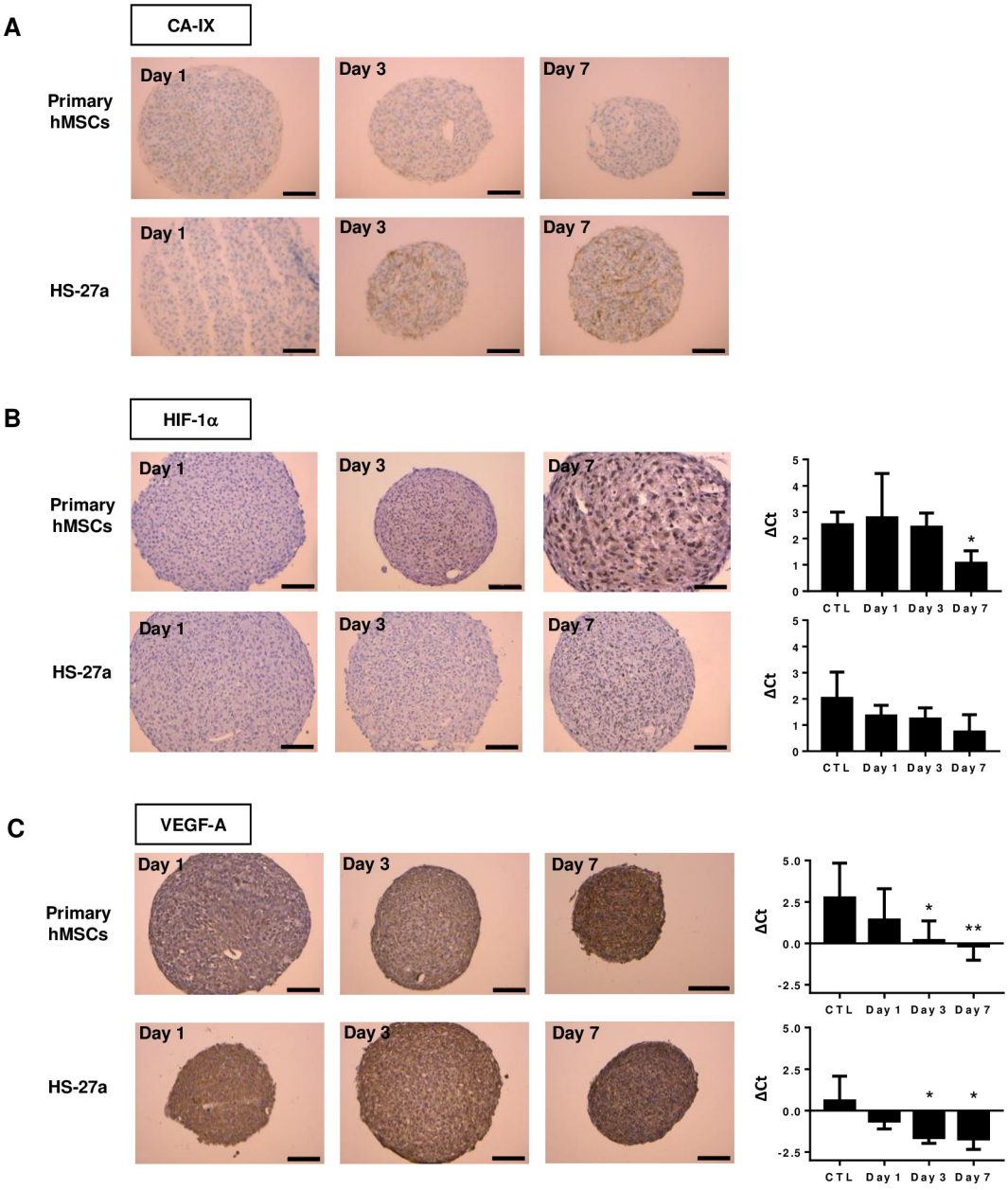

Fig 5. Hypoxia detection of primary hMSC- and HS-27a-spheroids over 7 days in culture. (A) Immunohistochemistry of CA-IX. (B) Immunohistochemistry and mRNA of HIF-1α. (C) Immunohistochemistry and mRNA expression of VEGF-A. (primary hMSCs n = 5; HS-27a n = 3; * $p \leq 0.05$; ** $p \leq 0.01$; scale bars = 100 μm).

https://doi.org/10.1371/journal.pone.0225485.g005

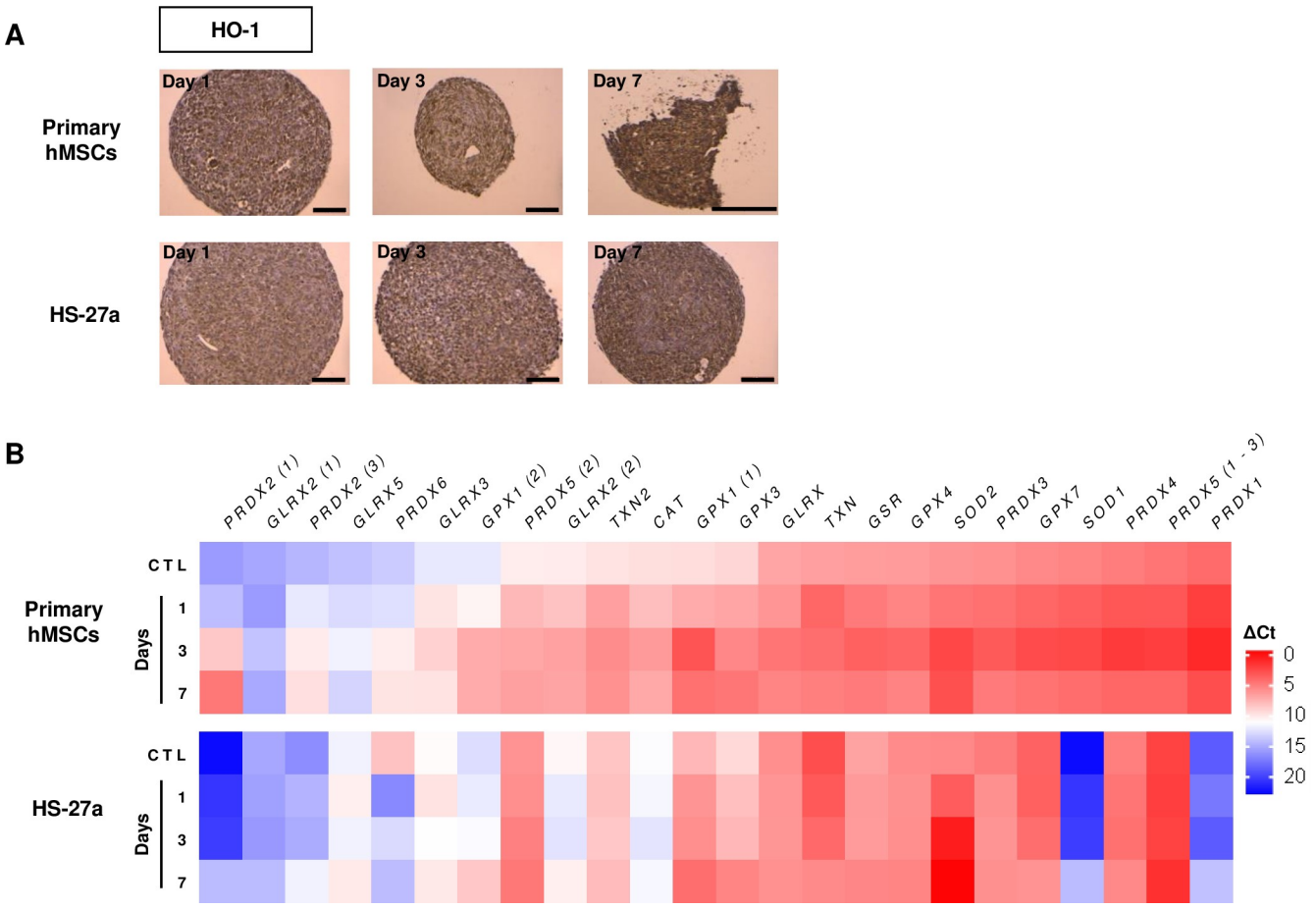

Fig 6. Oxidative stress detection in primary hMSC- and HS-27a-spheroids. (A) Immunohistochemistry of HO-1 (scale bars = 100 μm). (B) Expression of antioxidant genes (n = 3; data are mean; * compared to 2D control (CTL); * $p \leq 0.05$; ** $p \leq 0.01$).

https://doi.org/10.1371/journal.pone.0225485.g006

oxygen species (ROS). Heme oxygenase 1 (HO-1) is induced by a variety of stressors, and is therefore a marker of hypoxia and oxidative stress [48,51]. Indeed, oxidative stress triggers nuclear relocation of NRF-2, a HO-1 transcription factor, which then leads to antioxidant response through induced expression of antioxidants by HO-1. In the spheroids, we observed a high expression of HO-1 at day 1, which increased over time (Fig 6A). Conversely, among the 24 antioxidant genes [52], we found a total of seven genes upregulated in spheroids from the primary hMSCs and the HS-27a cell line (Fig 6B). Remarkably, of these genes, four (*GPX1*, *PRDX2*, *SOD1* and *SOD2*) were commonly upregulated in both cell types irrespective of their initial expression level.

Together, these data indicate concomitant appearance of hypoxia and oxidative stress in both primary hMSC- and HS-27a-spheroids, which could therefore explain initial cell cycle arrest and further apoptosis in prolonged hypoxia.

Dedifferentiation in MSC-spheroids

The 2D culture of MSCs critically leads to rapid loss of pluripotency after few passages, whereas MSC-spheroids can induce dedifferentiation, demonstrated by the expression of three pluripotent transcription factors (OCT-4, SOX-2 and NANOG) [32,53]. Furthermore, it has been described that hypoxia transcriptionally regulates these factors in a HIFs-dependent

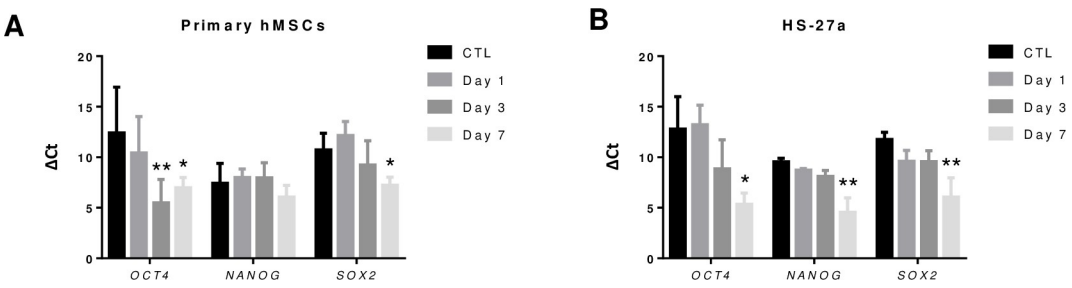

Fig 7. Dedifferentiation detection of hMSC- and HS-27a-spheroids over 7 days in culture. (A and B) Gene expression of *OCT4*, *NANOG* and *SOX2* for (A) primary hMSC- and (B) HS-27a-spheroids (primary hMSCs n = 5; HS-27a n = 3; * $p \leq 0.05$; ** $p \leq 0.01$).

https://doi.org/10.1371/journal.pone.0225485.g007

manner [54]. Therefore, in order to validate whether HS-27a behave similarly to primary hMSCs, we examined the expression of *OCT*-4, *SOX*-2 and *NANOG*, over time. Results showed that hMSC-spheroid formation was accompanied by upregulation of *OCT4* and *SOX2*, in agreement with previous studies, but surprisingly showed no upregulation of *NANOG* (Fig 7A). HS-27a had similar expression level of the three genes to hMSCs in 2D culture and had progressive increased expression of all markers, suggesting that the HS-27a retains dedifferentiation capacity like primary hMSCs (Fig 7B).

Discussion

MSC-spheroids have mainly been designed to study biological processes such as those related to *ex vivo* stem cell maintenance, differentiation capacity, immunity or anti-inflammatory, with the aim to improve their use in regenerative medicine [25,55]. For instance, studies have demonstrated the benefit of using MSC-spheroids in treating cardiac, cerebral, kidney and hindlimb ischemia [56–59] or in tissue cartilage and bone repair [60–63]. MSCs are also highly involved in hematopoietic homeostasis [1,10]. However, until recently, they were viewed as rare heterogeneous populations lining vessels in the BM. Using multiscale 3D quantitative microscopy, Gomariz *et al*. have elegantly revealed that mesenchymal reticular subsets are remarkably more abundant than previously estimated [64]. This reinforces the interest of studying MSCs in the hematopoietic context and investigating them from a 3D angle.

Many studies have examined complex matrix-based 3D models, while ultimately, only few have approached MSC-spheroids as *in vitro* surrogate of the hematopoietic niche. In brief, HSCs can migrate and settle into MSC-spheroids that provide higher potential to promote HSCs expansion and stemness maintenance, compared to 2D co-cultures [18,19]. Direct intra-bone delivery of MSC-spheroids containing HSCs also sustained higher engraftment and retention of HSCs compared to injected HSCs [17]. However, Schmal *et al*. drew our attention on the fact that hanging drop method led to lower proliferation of hematopoietic cells and decreased generation of progenitors compared to 2D co-culture, although the stem cell capability has not been yet tested [35]. These contrary data suggest that spheroid colonization by HSCs may certainly depend on the method used to create spheroids. Spheroids are also attractive tools to uncover mechanisms by which malignant cells remodel their microenvironment and MSCs participate in chemoresistance and relapse [65]. As a proof of concept, Reagan *et al*. showed that MSC-spheroids help to unravel mechanisms of regulation of osteoblasts in multiple myeloma [66], while Aljitawi *et al*. demonstrated that chemotherapy is linked to the expression of N-cadherin in AML [23].

Although MSC-spheroids appear to be a promising tool, studies might have been limited by the availability of primary hMSCs and the reproducibility due to different sources. Strangely,

2D co-cultures with hematopoietic cells have long been established with cell lines, mostly murine, such as MS-5 or M2-10B4 [11], but they have almost never been used to create 3D aggregates. Our study provides an evaluation of the ability of three cell lines to form spheroids. We chose HS-27a and HS-5 cell lines for their human origin and their known capacity to sustain hematopoiesis [38]. The HS-5 cells are described as fibroblastoid cells, secreting high amount of growth factors that support hematopoietic progenitors proliferation. The HS-27a cell line has epithelioid morphology, producing low level of growth factors but supporting hemapoietic stem cells [38]. Unlike MS-5 cells, HS-5 and HS-27a cells do not retain contact inhibition that certainly, although of human origin, have limited their use for long-term cultures. Independently of the contact inhibition capacity, the three cell lines were able to provide quick and reproducible spheroids. The delay to achieve a complete spheroid, compared to primary hMSCs, could certainly be attributed to sedimentation speed, cell lines being much smaller than primaries that could hence sediment faster. In agreement with previous studies [18], we found that primary hMSCs provide highly cohesive spheroids with a smooth surface. MS-5 had a similar appearance, whereas spheroids from human cell lines were more disorganized with distinct cells at the surface. ECM deposition was visible for all types of spheroids but ECM composition could differ, and the higher proliferation of human cell lines, which certainly induces ECM remodeling, may explain the differences.

Contrary to primary hMSC-spheroids, all spheroids from cell lines kept a constant size over time. This could be partially explained for human cells by the fact that cell lines continue to proliferate in spheroid culture, whereas primary MSCs are mostly quiescent, and may compensate cell death. However, HS-27a showed a decrease in viable cells similarly to primary hMSCs and MS-5 are quiescent but do not shrink. Shrinking has already been reported for primary hMSCs [31,32,35,37,67–69] and has been attributed to autophagy [32]. Reduced cell growth or arrest is known to trigger autophagy [70]. Since, HS-27a and HS-5 cell lines proliferate until 7 days in spheroids, one could hypothesize that transformed cell lines may have lower autophagy, contrary to quiescent primary hMSCs. Consistent with this assumption, TEM revealed high amounts of cytoplasmic vacuoles and autophagosomes in primary hMSC-spheroids, as early as day 1. Although cytoplasmic vacuoles progressively appeared in spheroid from cell lines, almost no autophagosomes were detected. It is worth noting that HS-27a and HS-5 were obtained from primary hMSCs transformed with Human papillomavirus 16E6/E7, which activates autophagy via Atg9B and LAMP1 in cervical cancer cells [71]. However, neither TEM, nor LC3B staining showed autophagy in HS-27a cells. Indeed, LC3B expression was strongly induced in HS-27a cells, which indicates response to stress and induction of the autophagic process, but staining remains diffuse in the cytoplasm, suggesting a blockage of the autophagy process. However, diffuse LC3B staining may hamper the interpretation in IHC, while a dot-like staining patterns is more indicative of autophagy [41]. Dots may also reflect the accumulation of autophagosomes due to induction of autophagy, or due to inhibition of autophagy resulting from a lack of autophagosome degradation upon fusion with lysosomes [72]. In the absence of obvious autophagy in cell lines, cell death could therefore be explained by necrosis, as shown by SEM, and apoptosis observed by caspase-3 staining in IHC (early apoptosis) and 7-AAD staining in flow cytometry (late apoptosis and necrosis). Low apoptosis is detected for primary hMSC-spheroids, but massive lysed and necrotic cells are seen by SEM as early as day 1, in addition to autophagy. In agreement with our results, others studies have also demonstrated induction of apoptosis after several days [35,67,73]. While MS-5 cells resemble primary cells with low proliferation and strongly increased cell death, probably due to their contact inhibition, they conversely did not shrink like human cell lines, probably because of low or no autophagy.

Strong hypoxia and oxidative stress are among the stressors that could have induced autophagy and/or apoptosis in spheroids. Oxygen gradients have been frequently reported in tumor-spheres, with deep hypoxia surrounding a necrotic core [44–46], as well as in MSC-spheroids [47]. The hypoxia response mainly occurs through the stabilization of hypoxia-inducible factors (HIFs), which are regulators of multiple biological processes, such as angiogenesis or energetic metabolism. HIFs have an essential pro-survival role by promoting genes, such as those involved in metabolism and autophagy [50]. However, acute and prolonged hypoxia may also trigger cell death through blocking DNA replication and induced oxidative stress [44,46]. In MSC-spheroids, we found increased expression of hypoxia markers, including HIF-1α and its target CA-IX, VEGF-A, concomitant to induced oxidative stress, as revealed by increased expression of HO-1 and the antioxidant response. *SOD2* and *GPX1* were the two genes with the greatest upregulation, which indicates strong oxidative stress. Interestingly, although HO-1 and antioxidant genes are typically NRF-2 targets, they could also be regulated by HIFs. Altogether, these data indicate appearance of hypoxia and oxidative stress in primary hMSC- and HS-27a-spheroids, which could therefore explain cell cycle arrest, induction of autophagy and further apoptosis in prolonged hypoxia.

The 2D culture of MSCs critically leads to rapid loss of pluripotency after few passages, whereas 3D culture has showed greater MSC stemness maintenance, and induced dedifferentiation, demonstrated by the expression of three pluripotent transcription factors (OCT-4, SOX-2 and NANOG) and multipotent differentiation capacity [32,43,53,74]. It is worth noting that hypoxia favors stemness and dedifferentiation and induces expression of pluripotent transcription factors through HIFs [75,76]. Like primary hMSC-spheroids, HS-27a-spheroids had increased expression of pluripotent markers. This confirmed that HS-27a behave similarly to primary hMSCs and had preserved dedifferentiation capacity that could also be (re)activated during spheroid formation.

Conclusions

Overall our data indicate that, like hMSCs, MSC cell lines can be used to make reproductible and easily handled spheroids. HS-27a cells resemble primary cells, and are of a particular interest for further studies, since they provide better support to HSCs compared to HS-5 cells [38–40]. Thus, this model could help in understanding mechanisms involved in MSC physiology and may be a simple model to study cell interactions in the hematopoietic niche. The model could also be extended to research metastatic process as previously described for breast cancer [28].

Supporting information

S1 Fig. Spheroids formation of mouse MS-5 cell line. (A and B) Scanning electron microscopy (SEM) analysis over 14 days (scale bars = 100 μm (A) and 20 μm (B). (C) Sub-G_1 apoptosis quantification (n = 3) and (D) cell cycle quantification over 21 days in culture (n = 3; data are mean ± SD).
(TIF)

S2 Fig. Transmission electron microscopy (TEM) observation of MSC-spheroids. TEM analysis of primary hMSC-spheroids at day 1 (A), day 3 (B) and day 7 (C); Higher magnification is also shown to highlight autophagosomes. HS-27a-spheroids at day 1 (D), day 3 (E) and day 7 (F); HS-5-spheroids at day 1 (G), day 3 (H) and day 7 (I) and MS-5-spheroids at day 1 (J), day 3 (K) and day 7 (L). Scale bars = 20 μm.
(PPTX)

S3 Fig. LC3B expression in HS-27a-spheroids. Immunohistochemistry of LC3B is shown at days 1, 3 and 7 for HS-27a-spheroids (scale bars = 50 μm).
(TIF)

S1 Video. A representative time-lapse video of spheroid formation. 30 000 primary MSCs seeded into U-bottomed 96-well, in medium containing 0.5% of methylcellulose (Methocult™ SF H4236) were followed via a Nikon Eclipse TI-S microscope for 24 hours.
(MP4)

S2 Video. A representative time-lapse video of spheroid formation. 30 000 HS-27a cells seeded into U-bottomed 96-well, in medium containing 0.5% of methylcellulose (Methocult™ SF H4236) were followed via a Nikon Eclipse TI-S microscope for 24 hours.
(MP4)

S3 Video. A representative time-lapse video of spheroid formation. 30,000 HS-5 cells seeded into U-bottomed 96-well, in medium containing 0.5% of methylcellulose (Methocult™ SF H4236) were followed via a Nikon Eclipse TI-S microscope for 24 hours.
(MP4)

S4 Video. A representative time-lapse video of spheroid formation. 30,000 MS-5 cells seeded into U-bottomed 96-well, in medium containing 0.5% of methylcellulose (Methocult™ SF H4236) were followed via a Nikon Eclipse TI-S microscope for 24 hours.
(MP4)

S1 Table. List of primers and probes sequences.
(DOCX)

Acknowledgments

We would like to thank P. G. Genever (University of York, UK) for providing valuable support, providing protocol and recommendations to establish spheroids. We also thank Sophie Hamard (University of Tours, France) for her technical assistance.

Author Contributions

Conceptualization: Frédéric Mazurier.

Data curation: Margaux Deynoux, Nicola Sunter, Gaëlle Fromont, Frédéric Mazurier.

Formal analysis: Margaux Deynoux, Nicola Sunter, Hassan Dakik, Florence Rouleux-Bonnin, Philippe Roingeard, Gaëlle Fromont.

Funding acquisition: Olivier Hérault, Frédéric Mazurier.

Investigation: Margaux Deynoux, Nicola Sunter, Elfi Ducrocq, Hassan Dakik, Roseline Guibon, Julien Burlaud-Gaillard.

Methodology: Margaux Deynoux, Nicola Sunter, Elfi Ducrocq, Hassan Dakik, Roseline Guibon, Julien Burlaud-Gaillard, Lucie Brisson, Frédéric Mazurier.

Project administration: Frédéric Mazurier.

Resources: Louis-Romée le Nail, Olivier Hérault, Jorge Domenech, Gaëlle Fromont.

Supervision: Philippe Roingeard, Gaëlle Fromont, Frédéric Mazurier.

Validation: Margaux Deynoux, Nicola Sunter, Philippe Roingeard, Gaëlle Fromont, Frédéric Mazurier.

Writing – original draft: Margaux Deynoux, Nicola Sunter, Frédéric Mazurier.

Writing – review & editing: Margaux Deynoux, Nicola Sunter, Hassan Dakik, Roseline Guibon, Julien Burlaud-Gaillard, Lucie Brisson, Florence Rouleux-Bonnin, Olivier Hérault, Jorge Domenech, Philippe Roingeard, Gaëlle Fromont, Frédéric Mazurier.

References

1. Domenech J. What Are Mesenchymal Stromal Cells? Origin and Discovery of Mesenchymal Stromal Cells. In: Mesenchymal Stromal Cells as Tumor Stromal Modulators. 2017. p. 1–37.
2. Dominici M, Le Blanc K, Mueller I, Slaper-Cortenbach I, Marini F, Krause D, et al. Minimal criteria for defining multipotent mesenchymal stromal cells. The International Society for Cellular Therapy position statement. Cytotherapy. 2006; 8(4):315–7. https://doi.org/10.1080/14653240600855905 PMID: 16923606
3. Makino S, Fukuda K, Miyoshi S, Konishi F, Kodama H, Pan J, et al. Cardiomyocytes can be generated from marrow stromal cells in vitro. J Clin Invest. 1999; 103(5):697–705. https://doi.org/10.1172/JCI5298 PMID: 10074487
4. Sanchez-Ramos J, Song S, Cardozo-Pelaez F, Hazzi C, Stedeford T, Willing A, et al. Adult bone marrow stromal cells differentiate into neural cells in vitro. Exp Neurol. 2000; 164(2):247–56. https://doi.org/10.1006/exnr.2000.7389 PMID: 10915564
5. Spees JL, Olson SD, Ylostalo J, Lynch PJ, Smith J, Perry A, et al. Differentiation, cell fusion, and nuclear fusion during ex vivo repair of epithelium by human adult stem cells from bone marrow stroma. Proc Natl Acad Sci. 2003; 100(5):2397–402. https://doi.org/10.1073/pnas.0437997100 PMID: 12606728
6. Hong SH, Gang EJ, Jeong JA, Ahn C, Hwang SH, Yang IH, et al. In vitro differentiation of human umbilical cord blood-derived mesenchymal stem cells into hepatocyte-like cells. Biochem Biophys Res Commun. 2005; 330(4):1153–61. https://doi.org/10.1016/j.bbrc.2005.03.086 PMID: 15823564
7. Yan L, Zheng D, Xu RH. Critical role of tumor necrosis factor signaling in mesenchymal stem cell-based therapy for autoimmune and inflammatory diseases. Front Immunol. 2018; 9:1658. https://doi.org/10.3389/fimmu.2018.01658 PMID: 30079066
8. Su P, Tian Y, Yang C, Ma X, Wang X, Pei J, et al. Mesenchymal stem cell migration during bone formation and bone diseases therapy. Int J Mol Sci. 2018; 19(8):E2343. https://doi.org/10.3390/ijms19082343 PMID: 30096908
9. Perez JR, Kouroupis D, Li DJ, Best TM, Kaplan L, Correa D. Tissue Engineering and Cell-Based Therapies for Fractures and Bone Defects. Front Bioeng Biotechnol. 2018; 6(105):1–23.
10. Pinho S, Frenette PS. Haematopoietic stem cell activity and interactions with the niche. Nat Rev Mol Cell Biol. 2019; 20(5):303–20. https://doi.org/10.1038/s41580-019-0103-9 PMID: 30745579
11. Vaidya A, Kale V. Hematopoietic stem cells, their niche, and the concept of co-culture systems: A critical review. J Stem Cells. 2015; 10(1):13–31. PMID: 26665935
12. Dhami SPS, Kappala SS, Thompson A, Szegezdi E. Three-dimensional ex vivo co-culture models of the leukaemic bone marrow niche for functional drug testing. Drug Discov Today. 2016; 21(9):1464–71. https://doi.org/10.1016/j.drudis.2016.04.019 PMID: 27130156
13. Cesarz Z, Tamama K. Spheroid Culture of Mesenchymal Stem Cells. Stem Cells Int. 2016; 2016: e9176357.
14. Lin RZ, Chang HY. Recent advances in three-dimensional multicellular spheroid culture for biomedical research. Biotechnol J. 2008; 3(9–10):1172–84. https://doi.org/10.1002/biot.200700228 PMID: 18566957
15. Baraniak PR, McDevitt TC. Scaffold-free culture of mesenchymal stem cell spheroids in suspension preserves multilineage potential. Cell Tissue Res. 2012; 347(3):701–11. https://doi.org/10.1007/s00441-011-1215-5 PMID: 21833761
16. Ghazanfari R, Li H, Zacharaki D, Lim HC, Scheding S. Human Non-Hematopoietic CD271pos/CD140a-low/neg Bone Marrow Stroma Cells Fulfill Stringent Stem Cell Criteria in Serial Transplantations. Stem Cells Dev. 2016; 25(21):1652–8. https://doi.org/10.1089/scd.2016.0169 PMID: 27527928
17. Futrega K, Atkinson K, Lott WB, Doran MR. Spheroid Coculture of Hematopoietic Stem/Progenitor Cells and Monolayer Expanded Mesenchymal Stem/Stromal Cells in Polydimethylsiloxane Microwells Modestly Improves In Vitro Hematopoietic Stem/Progenitor Cell Expansion. Tissue Eng Part C Methods. 2017; 23(4):200–18. https://doi.org/10.1089/ten.tec.2016.0329 PMID: 28406754

18. De Barros APDN, Takiya CM, Garzoni LR, Leal-Ferreira ML, Dutra HS, Chiarini LB, et al. Osteoblasts and bone marrow mesenchymal stromal cells control hematopoietic stem cell migration and proliferation in 3D in vitro model. PLoS One. 2010; 5(2):e9093. https://doi.org/10.1371/journal.pone.0009093 PMID: 20161704

19. Isern J, Martín-Antonio B, Ghazanfari R, Martín AM, López JA, DelToro R, et al. Self-Renewing Human Bone Marrow Mesenspheres Promote Hematopoietic Stem Cell Expansion. Cell Rep. 2013; 3(5):1714–24. https://doi.org/10.1016/j.celrep.2013.03.041 PMID: 23623496

20. Bruce A, Evans R, Mezan R, Shi L, Moses BS, Martin KH, et al. Three-dimensional microfluidic tri-culture model of the bone marrow microenvironment for study of acute lymphoblastic leukemia. PLoS One. 2015; 10(10):e0140506. https://doi.org/10.1371/journal.pone.0140506 PMID: 26488876

21. Wuchter P, Saffrich R, Giselbrecht S, Nies C, Lorig H, Kolb S, et al. Microcavity arrays as an in vitro model system of the bone marrow niche for hematopoietic stem cells. Cell Tissue Res. 2016; 364 (3):573–84. https://doi.org/10.1007/s00441-015-2348-8 PMID: 26829941

22. Leisten I, Kramann R, Ventura Ferreira MS, Bovi M, Neuss S, Ziegler P, et al. 3D co-culture of hematopoietic stem and progenitor cells and mesenchymal stem cells in collagen scaffolds as a model of the hematopoietic niche. Biomaterials. 2012; 33(6):1736–47. https://doi.org/10.1016/j.biomaterials.2011.11.034 PMID: 22136713

23. Aljitawi OS, Li D, Xiao Y, Zhang D, Ramachandran K, Stehno-Bittel L, et al. A novel three-dimensional stromal-based model for in vitro chemotherapy sensitivity testing of leukemia cells. Leuk Lymphoma. 2014; 55(2):378–91. https://doi.org/10.3109/10428194.2013.793323 PMID: 23566162

24. Sart S, Tsai A-C, Li Y, Ma T. Three-dimensional aggregates of mesenchymal stem cells: cellular mechanisms, biological properties, and applications. Tissue Eng Part B Rev. 2014; 20(5):365–80. https://doi.org/10.1089/ten.TEB.2013.0537 PMID: 24168395

25. Egger D, Tripisciano C, Weber V, Dominici M, Kasper C. Dynamic Cultivation of Mesenchymal Stem Cell Aggregates. Bioengineering. 2018; 5(2):1–15.

26. Ong SM, Zhang C, Toh YC, Kim SH, Foo HL, Tan CH, et al. A gel-free 3D microfluidic cell culture system. Biomaterials. 2008; 29(22):3237–44. https://doi.org/10.1016/j.biomaterials.2008.04.022 PMID: 18455231

27. Saleh FA, Frith JE, Lee JA, Genever PG. Three-Dimensional In Vitro Culture Techniques for Mesenchymal Stem Cells. In: Progenitor Cells: Methods and Protocols. 2012. p. 31–45.

28. Cavnar SP, Rickelmann AD, Meguiar KF, Xiao A, Dosch J, Leung BM, et al. Modeling Selective Elimination of Quiescent Cancer Cells from Bone Marrow. Neoplasia. 2015; 17(8):625–33. https://doi.org/10.1016/j.neo.2015.08.001 PMID: 26408255

29. Itoh K, Tezuka H, Sakoda H, Konno M, Nagata K, Uchiyama T, et al. Reproducible establishment of hemopoetic supportive stromal cell lines from murine bone marrow. Exp Hematol. 1989; 17(2):145–53. PMID: 2783573

30. Saleh FA, Whyte M, Genever PG. Effects of endothelial cells on human mesenchymal stem cell activity in a three-dimensional in vitro model. Eur Cells Mater. 2011; 22:242–57.

31. Shearier E, Xing Q, Qian Z, Zhao F. Physiologically Low Oxygen Enhances Biomolecule Production and Stemness of Mesenchymal Stem Cell Spheroids. Tissue Eng Part C. 2016; 22(4):360–9.

32. Pennock R, Bray E, Pryor P, James S, McKeegan P, Sturmey R, et al. Human cell dedifferentiation in mesenchymal condensates through controlled autophagy. Sci Rep. 2015; 5:e13113.

33. Matak D, Brodaczewska KK, Lipiec M, Szymanski Ł, Szczylik C, Czarnecka AM. Colony, hanging drop, and methylcellulose three dimensional hypoxic growth optimization of renal cell carcinoma cell lines. Cytotechnology. 2017; 69(4):565–78. https://doi.org/10.1007/s10616-016-0063-2 PMID: 28321776

34. Foty R. A Simple Hanging Drop Cell Culture Protocol for Generation of 3D Spheroids. J Vis Exp. 2011; 20(51):1–4.

35. Schmal O, Seifert J, Schäffer T, Walter CB, Aicher WK, Klein G. Hematopoietic Stem and Progenitor Cell Expansion in Contact with Mesenchymal Stromal Cells in a Hanging Drop Model Uncovers Disadvantages of 3D. Stem Cells Int. 2015; 2016:e4148093.

36. Blocki A, Wang Y, Koch M, Peh P, Beyer S, Law P, et al. Not All MSCs Can Act as Pericytes: Functional In Vitro Assays to Distinguish Pericytes from Other Mesenchymal Stem Cells in Angiogenesis. Stem Cells Dev. 2013; 22(17):2347–55. https://doi.org/10.1089/scd.2012.0415 PMID: 23600480

37. Redondo-Castro E, Cunningham CJ, Miller J, Cain S, Allan SM, Pinteaux E. Generation of Human Mesenchymal Stem Cell 3D Spheroids Using Low-binding Plates. Bio Protoc. 2018; 8(16):e2968. https://doi.org/10.21769/BioProtoc.2968 PMID: 30294619

38. Roecklein BA, Torok-Storb B. Functionally distinct human marrow stromal cell lines immortalized by transduction with the human papilloma virus E6/E7 genes. Blood. 1995; 85(4):997–1005. PMID: 7849321

39. Torok-Storb B, Iwata M, Graf L, Gianotti J, Horton H, Byrne MC. Dissecting the marrow microenvironment. In: Annals of the New York Academy of Sciences. 1999. p. 164–70.

40. Iwata M, Sandstrom RS, Delrow JJ, Stamatoyannopoulos JA, Torok-Storb B. Functionally and phenotypically distinct subpopulations of marrow stromal cells are fibroblast in origin and induce different fates in peripheral blood monocytes. Stem Cells Dev. 2014; 23(7):729–40. https://doi.org/10.1089/scd.2013.0300 PMID: 24131213

41. Klionsky DJ, Abdelmohsen K, Abe A, Abedin MJ, Abeliovich H, Arozena AA, et al. Guidelines for the use and interpretation of assays for monitoring autophagy (3rd edition). Autophagy. 2016; 12(1):1–222. https://doi.org/10.1080/15548627.2015.1100356 PMID: 26799652

42. Schläfli AM, Berezowska S, Adams O, Langer R, Tschan MP. Reliable LC3 and p62 autophagy marker detection in formalin fixed paraffin embedded human tissue by immunohistochemistry. Eur J Histochem. 2015; 59(2):2481. https://doi.org/10.4081/ejh.2015.2481 PMID: 26150155

43. Li Y, Guo G, Li L, Chen F, Bao J, Shi Y jun, et al. Three-dimensional spheroid culture of human umbilical cord mesenchymal stem cells promotes cell yield and stemness maintenance. Cell Tissue Res. 2015; 360(2):297–307. https://doi.org/10.1007/s00441-014-2055-x PMID: 25749992

44. Riffle S, Hegde RS. Modeling tumor cell adaptations to hypoxia in multicellular tumor spheroids. J Exp Clin Cancer Res. 2017; 36(1):e102.

45. Leek R, Grimes DR, Harris AL, McIntyre A. Methods: Using Three-Dimensional Culture (Spheroids) as an In Vitro Model of Tumour Hypoxia. In: Tumor microenvironment. 2016. p. 167–96.

46. Riffle S, Pandey RN, Albert M, Hegde RS. Linking hypoxia, DNA damage and proliferation in multicellular tumor spheroids. BMC Cancer. 2017; 17(1):1–12. https://doi.org/10.1186/s12885-016-3022-6

47. Sharma MB, Limaye LS, Kale VP. Mimicking the functional hematopoietic stem cell niche in vitro: Recapitulation of marrow physiology by hydrogel-based three-dimensional cultures of mesenchymal stromal cells. Haematologica. 2012; 97(5):651–60. https://doi.org/10.3324/haematol.2011.050500 PMID: 22058199

48. Potapova IA, Gaudette GR, Brink PR, Robinson RB, Rosen MR, Cohen IS, et al. Mesenchymal Stem Cells Support Migration, Extracellular Matrix Invasion, Proliferation, and Survival of Endothelial Cells In Vitro. Stem Cells. 2007; 25(7):1761–8. https://doi.org/10.1634/stemcells.2007-0022 PMID: 17395769

49. McDonald PC, Dedhar S. Carbonic anhydrase IX (CAIX) as a mediator of hypoxia-induced stress response in cancer cells. In: SubCellular Biochemistry. 2014. p. 255–69.

50. Zhang CC, Sadek HA. Hypoxia and Metabolic Properties of Hematopoietic Stem Cells. Antioxid Redox Signal. 2014; 20(12):1891–901. https://doi.org/10.1089/ars.2012.5019 PMID: 23621582

51. Dunn LL, Midwinter RG, Ni J, Hamid HA, Parish CR, Stocker R. New insights into intracellular locations and functions of heme oxygenase-1. Antioxidants Redox Signal. 2014; 20(11):1723–42.

52. Picou F, Vignon C, Debeissat C, Lachot S, Kosmider O, Gallay N, et al. Bone marrow oxidative stress and specific antioxidant signatures in myelodysplastic syndromes. Blood Adv. 2019; 3(24):4271–9. https://doi.org/10.1182/bloodadvances.2019000677 PMID: 31869414

53. Zhang Q, Nguyen AL, Shi S, Hill C, Wilder-Smith P, Krasieva TB, et al. Three-dimensional spheroid culture of human gingiva-derived mesenchymal stem cells enhances mitigation of chemotherapy-induced oral mucositis. Stem Cells Dev. 2012; 21(6):937–47. https://doi.org/10.1089/scd.2011.0252 PMID: 21689066

54. Drela K, Sarnowska A, Siedlecka P, Szablowska-Gadomska I, Wielgos M, Jurga M, et al. Low oxygen atmosphere facilitates proliferation and maintains undifferentiated state of umbilical cord mesenchymal stem cells in an hypoxia inducible factor-dependent manner. Cytotherapy. 2014; 16(7):881–92. https://doi.org/10.1016/j.jcyt.2014.02.009 PMID: 24726658

55. Xie L, Mao M, Zhou L, Jiang B. Spheroid Mesenchymal Stem Cells and Mesenchymal Stem Cell-Derived Microvesicles: Two Potential Therapeutic Strategies. Stem Cells Dev. 2016; 25(3):203–13. https://doi.org/10.1089/scd.2015.0278 PMID: 26575103

56. Ceccaldi C, Bushkalova R, Alfarano C, Lairez O, Calise D, Bourin P, et al. Evaluation of polyelectrolyte complex-based scaffolds for mesenchymal stem cell therapy in cardiac ischemia treatment. Acta Biomater. 2014; 10(2):901–11. https://doi.org/10.1016/j.actbio.2013.10.027 PMID: 24211733

57. Bhang SH, Lee S, Shin J-Y, Lee T-J, Kim B-S. Transplantation of Cord Blood Mesenchymal Stem Cells as Spheroids Enhances Vascularization. Tissue Eng Part A. 2012; 18(19–20):2138–47. https://doi.org/10.1089/ten.TEA.2011.0640 PMID: 22559333

58. Guo L, Ge J, Zhou Y, Wang S, Zhao RCH, Wu Y. Three-Dimensional Spheroid-Cultured Mesenchymal Stem Cells Devoid of Embolism Attenuate Brain Stroke Injury After Intra-Arterial Injection. Stem Cells Dev. 2013; 23(9):978–89.

59. Xu Y, Shi T, Xu A, Zhang L. 3D spheroid culture enhances survival and therapeutic capacities of MSCs injected into ischemic kidney. J Cell Mol Med. 2016; 20(7):1203–13. https://doi.org/10.1111/jcmm.12651 PMID: 26914637

60. Yamaguchi Y, Ohno J, Sato A, Kido H, Fukushima T. Mesenchymal stem cell spheroids exhibit enhanced in-vitro and in-vivo osteoregenerative potential. BMC Biotechnol. 2014; 14(105):1–10.

61. Ma D, Zhong C, Yao H, Liu Y, Chen F, Li J, et al. Engineering injectable bone using bone marrow stromal cell aggregates. Stem Cells Dev. 2011; 20(6):989–99. https://doi.org/10.1089/scd.2010.0348 PMID: 21091305

62. Suzuki S, Muneta T, Tsuji K, Ichinose S, Makino H, Umezawa A, et al. Properties and usefulness of aggregates of synovial mesenchymal stem cells as a source for cartilage regeneration. Arthritis Res Ther. 2012; 14(3):R136. https://doi.org/10.1186/ar3869 PMID: 22676383

63. Suenaga H, Furukawa KS, Suzuki Y, Takato T, Ushida T. Bone regeneration in calvarial defects in a rat model by implantation of human bone marrow-derived mesenchymal stromal cell spheroids. J Mater Sci Mater Med. 2015; 26(11):254. https://doi.org/10.1007/s10856-015-5591-3 PMID: 26449444

64. Gomariz A, Helbling PM, Isringhausen S, Suessbier U, Becker A, Boss A, et al. Quantitative spatial analysis of haematopoiesis-regulating stromal cells in the bone marrow microenvironment by 3D microscopy. Nat Commun. 2018; 9(1).

65. Medyouf H. The microenvironment in human myeloid malignancies: emerging concepts and therapeutic implications. Blood. 2017; 129(12):1617–26. https://doi.org/10.1182/blood-2016-11-696070 PMID: 28159735

66. Reagan MR, Mishima Y, Glavey S V, Zhang Y, Manier S, Lu ZN, et al. Investigating osteogenic differentiation in multiple myeloma using a novel 3D bone marrow niche model. Blood. 2014; 124(22):3250–9. https://doi.org/10.1182/blood-2014-02-558007 PMID: 25205118

67. Tsai A-C, Liu Y, Yuan X, Ma T. Compaction, fusion, and functional activation of three-dimensional human mesenchymal stem cell aggregate. Tissue Eng Part A. 2015; 21(9–10):1705–19. https://doi.org/10.1089/ten.TEA.2014.0314 PMID: 25661745

68. Kim M, Yun H, Young D, Byung P, Choi H. Three-Dimensional Spheroid Culture Increases Exosome Secretion from Mesenchymal Stem Cells. Tissue Eng Regen Med. 2018; 15(4):427–36. https://doi.org/10.1007/s13770-018-0139-5 PMID: 30603566

69. Bellotti C, Duchi S, Bevilacqua A, Lucarelli E, Piccinini F. Long term morphological characterization of mesenchymal stromal cells 3D spheroids built with a rapid method based on entry-level equipment. Cytotechnology. 2016;1–12.

70. Neufeld TP. Autophagy and cell growth—the yin and yang of nutrient responses. J Cell Sci. 2012; 125 (10):2359–68.

71. Tingting C, Shizhou Y, Songfa Z, Junfen X, Weiguo L, Xiaodong C, et al. Human papillomavirus 16E6/E7 activates autophagy via Atg9B and LAMP1 in cervical cancer cells. Cancer Med. 2019; 8(9):4404–16. https://doi.org/10.1002/cam4.2351 PMID: 31215164

72. Holt S V., Wyspianska B, Randall KJ, James D, Foster JR, Wilkinson RW. The development of an immunohistochemical method to detect the autophagy-associated protein LC3-II in human tumor xenografts. Toxicol Pathol. 2011; 39(3):516–23. https://doi.org/10.1177/0192623310396903 PMID: 21441228

73. Ho SS, Hung BP, Heyrani N, Lee MA, Leach JK. Hypoxic Preconditioning of Mesenchymal Stem Cells with Subsequent Spheroid Formation Accelerates Repair of Segmental Bone Defects. Stem Cells. 2018; 36(9):1393–403. https://doi.org/10.1002/stem.2853 PMID: 29968952

74. Cheng NC, Wang S, Young TH. The influence of spheroid formation of human adipose-derived stem cells on chitosan films on stemness and differentiation capabilities. Biomaterials. 2012; 33(6):1748–58. https://doi.org/10.1016/j.biomaterials.2011.11.049 PMID: 22153870

75. Park IH, Kim KH, Choi HK, Shim JS, Whang SY, Hahn SJ, et al. Constitutive stabilization of hypoxia-inducible factor alpha selectively promotes the self-renewal of mesenchymal progenitors and maintains mesenchymal stromal cells in an undifferentiated state. Exp Mol Med. 2013; 45(9):1–11.

76. Grayson WL, Zhao F, Bunnell B, Ma T. Hypoxia enhances proliferation and tissue formation of human mesenchymal stem cells. Biochem Biophys Res Commun. 2007; 358(3):948–53. https://doi.org/10.1016/j.bbrc.2007.05.054 PMID: 17521616